Available online at www.sciencedirect.com
SCIENCE DIRECT®
International Journal of Refractory Metals & Hard Materials 23 (2005) 161–170
International Journal of REFRACTORY METALS & HARD MATERIALS
www.elsevier.com/locate/ijrmhm

Infrared brazing Ti–6Al–4V and Mo using the Ti–15Cu–15Ni braze alloy

C.T. Chang [a,*], R.K. Shiue [b]

[a] Department of Materials Science and Engineering, National Dong Hwa University, Hualien 974, Taiwan
[b] Department of Materials Science and Engineering, National Taiwan University, Taipei 106, Taiwan

Received 1 November 2004; accepted 10 January 2005

Abstract

Brazing Ti–6Al–4V and Mo using the Ti–15Cu–15Ni alloy has been extensively evaluated in the study. Both infrared and conventional furnace brazing are included in the experiment. Ti–15Cu–15Ni braze alloy demonstrates excellent wettability on Ti–6Al–4V at 970 °C. In contrast, the wettability of the molten braze on the Mo substrate is significantly improved for the test temperature above 1000 °C. The brazed specimen is primarily comprised of the Ti-rich phase, and there is no interfacial reaction layer observed in the joint. Most of the brazed joints are fractured at the Mo substrate except for the joint infrared brazed at 970 °C for 180 s. For the specimen infrared brazed at 970 °C for 180 s demonstrates the average shear strength of 251 MPa, and quasi-cleavage fracture with sliding marks on facets is widely observed in the fractured surface. ABAQUS® stress simulations are also performed in order to illustrate the effect of residual stresses in the brazed joint during shear test. Based on the simulated result, there are two possible fracture locations in the brazed joint due to the presence of high Mises stresses, i.e., the braze alloy and Mo substrate. Additionally, the inherent low strength of the Mo substrate results in premature failure of the brazed joint during shear test for most brazed specimens.
© 2005 Elsevier Ltd. All rights reserved.

Keywords: Infrared brazing; Molybdenum; Ti–6Al–4V; Ti–15Cu–15Ni; Microstructure; Residual stresses; Shear test

1. Introduction

The titanium alloy has been used as the structural material since 1952 [1]. For the titanium alloy, V is typically added since it is an isomorphous β stabilizer. In contrast, the solubility of Al in Ti plays a crucial role of α stabilizer [2,3]. Accordingly, Ti–6Al–4V belongs to a type of α–β titanium alloys, which can be strengthened by various solution and aging treatments. The equilibrium of a single β phase is stable at high temperatures, and the α phase is transformed from the β phase at lower temperatures. With the proper heat treatment, the equilibrium phases for a wide composition range of α–β titanium alloys are mixture of α-Ti and β-Ti. Ti–6Al–4V has a large number of applications in the aerospace industry, mainly due to its superior strength to weight ratio [1]. Additionally, excellent corrosion resistance, good weldability, excellent elevated-temperature mechanical properties greatly promote applications of the Ti–6Al–4V alloy. It is by far the most important and widely used titanium alloy, accounting for about 60% of the titanium market [1].

The molybdenum metal belongs to refractory metals with the high melting point of 2610 °C [1]. Molybdenum has been used in the nuclear, chemical and defense industries [4]. However, mechanical properties of most refractory metals are greatly affected by their ductile-to-brittle transition behavior [1,4]. For example, the molybdenum is brittle at room temperature, and it must be brazed in a stress-free condition. The recrystallization temperature range of the unalloyed Mo is between 1150

* Corresponding author. Tel.: +886 3 8634209; fax: +886 3 8634200.
E-mail address: jct1028@ms41.hinet.net (C.T. Chang).

0263-4368/$ - see front matter © 2005 Elsevier Ltd. All rights reserved.
doi:10.1016/j.ijrmhm.2005.01.002

and 1200 °C [1,5]. If the maximum joint strength is required, the refractory metal must be brazed below its recrystallization temperature. Accordingly, this investigation is concentrated on infrared vacuum brazing of Ti–6Al–4V and Mo below the recrystallization temperature of molybdenum.

The titanium alloy has a high reactivity with many other elements. It can easily form oxide and nitride because of its high affinity to most interstitial elements such as oxygen, nitrogen... etc [1]. It is preferred that welding of titanium alloys be protected by inert gas or high vacuum environment. However, welding of Ti alloys may be not appropriate for all applications such as the component composed of dissimilar alloys [6]. Brazing is usually considered a good alternative method if the welding is inappropriate [7]. Selection of the filler metal used in brazing titanium alloy(s) always plays a crucial role in order to avoid formation of undesirable brittle intermetallics [6]. Ti–15Cu–15Ni in weight percent is a commercially available brazing filler metal, which can successfully braze many titanium alloys [6–8]. The service temperature of Ti–15Cu–15Ni alloy is as high as 870 °C, so the braze alloy is suitable for medium/high temperature applications [7].

The development of high-intensity infrared lamps and the availability of suitable reflectors have made infrared heating pragmatic for brazing [6]. Compared with the conventional vacuum furnace brazing, infrared vacuum brazing is characterized by a very rapid thermal history with the heating rate as high as 3000 °C/min [9–12]. Decreasing the brazing temperature and/or time are always recommended with the advantages of decreased interfacial reactions, decreased erosion of substrates and minimum loss of base metal properties [5,6,13]. Therefore, infrared brazing Ti–6Al–4V and Mo is primarily focused in the experiment in addition to conventional furnace brazing.

The finite element analysis (FEA) provides an alternative way to obtain solutions of practical engineering problems in different fields, e.g., solid mechanics, heat transfer and fluid mechanics...etc. The estimation of residual stresses in the brazed specimen is simulated by using a commercially available program, ABAQUS®. In this study, ABAQUS® simulation is applied in order to illustrate the effect of residual stresses in the brazed joint after the shear test experiment. Accordingly, the fracture mechanism of the brazed joint is also comprehensively discussed.

2. Experimental procedures

Base metals used in the test were pure molybdenum and Ti–6Al–4V plates with the dimension of $10 \times 10 \times 3$ mm, respectively. The brazed specimen was sectioned by a high-speed diamond saw. Brazed surfaces of both substrates were polished with SiC papers up to 1200 grit, and subsequently cleaned using an ultrasonic bath with acetone as the solvent prior to brazing. Ticuni® foil is the commercial product of Wesgo company, and its chemical composition in weight percent is 70%Ti, 15%Cu and 15%Ni. The solidus and liquidus temperature of Ticuni® foil are 910 °C and 960 °C, respectively [14]. It was in the form of foil with 100 mm wide and 50 μm thick.

Dynamic wetting angle measurements were performed using a conventional vacuum furnace with various temperatures for 0–2400 s [15,16]. The heating rate of the vacuum furnace was maintained at 30 °C/min, and the average cooling rate was approximately the same as heating rate. The braze alloy with near spherical shape used in the wetting angle test was prepared from Ticuni® foil by vacuum arc remelting (VAR) with an operation voltage of 60 V and a current of 130–150 A. The weight of each spherical ball was approximately 0.12 g [15,16]. In the wetting angle test, the spherical ball was placed on the molybdenum and Ti–6Al–4V substrates, respectively. The image of the molten braze on the substrate was recorded simultaneously using an Olympus C-5050 digital camera during the wetting angle measurement.

Both conventional furnace brazing and infrared brazing were performed in the experiment with a vacuum of 5×10^{-5} mbar at various specified temperatures. Infrared brazing was performed at 970, 1000, 1030 and 1060 °C for 180 and 300 s, respectively. The conventional furnace brazing was performed at 970 °C for 600, 1200 and 1800 s. Heating rates of infrared brazing and traditional furnace brazing were kept at 600 °C/min and 30 °C/min, respectively. Additionally, all brazed specimens were preheated at 600 °C for 600 s before the brazing temperature was attained. Table 1 summarizes all brazing conditions used in the study.

A standard metallographic procedure was applied to all brazed specimens prior to further microstructural inspections. Their cross sections were first ground by SiC papers, and subsequently polished by 0.05 μm alumina powder. Kroll's reagent (3 ml HF, 6 ml HNO_3 and 100 ml H_2O) was selected as the etching solution [17]. The cross section of the brazed specimen was examined using a Hitachi 3500H scanning electron microscope (SEM) equipped with an energy-dispersive X-ray spectrometer (EDS) for chemical analyses. The operational voltage was kept at 20 kV, and its spot size was approximately 1 μm.

The shear test was employed in order to evaluate the bonding strength of the brazed specimen [10,12,18,19]. Fig. 1 shows the schematic diagram of the shear test specimen used in this experiment. The middle shaded area is the Mo substrate, and two Ti–6Al–4V substrates are located at the outer shaded areas next to the molybdenum. The outer part of the layout is the specimen

Table 1
Summary of the process variables used in the experiment

Types of brazing	Brazing time (s)	Temperature			
		970 °C	1000 °C	1030 °C	1060 °C
Infrared brazing	180	S/M	S/M	S/M	S/M
Infrared brazing	300	M	M	M	M
Furnace brazing	600	M			
Furnace brazing	1200	S/M			
Furnace brazing	1800	M			
Furnace heating	0–2400	W	W	W	

S: shear test specimen, M: metallographic specimen, W: wetting angle measurement.

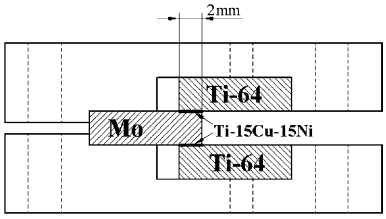

Fig. 1. Schematic diagram of the shear testing specimen.

holder used in brazing. Additionally, two bold black lines with 2.0 mm width in the middle of the graph indicate the location of Ti–15Cu–15Ni braze alloy. A Shimadzu AG-10 universal testing machine with a constant crosshead speed of 0.5 mm/min compressed the brazed specimen in the shear test [10,12]. Both the SEM cross-sectional image and fractographs of the brazed joint after shear test were examined in the experiment.

Evolution of the residual stress in the brazed joint can be simulated by using a finite element analysis (FEA) program, ABAQUS® [20]. ABAQUS® has been successfully applied in many engineering cases in previous studies [21–23]. The purpose of computer simulation is to verify the effect of shear test on the brazed joint for various brazing conditions. Accordingly, the maximum Mises stress is used in order to define the failure criteria of the brazed joint [20–23]. The failure mechanism of the brazed joint after shear test can be inferred by both ABAQUS® simulated result as well as SEM observations.

3. Results and discussion

3.1. Wetting angle tests of Ti–15Cu–15Ni on both substrates

Since the liquidus temperature of Ti–15Cu–15Ni alloy is 960 °C, the wetting angle test is performed above 960 °C. Based on the wetting angle measurement result, Ti–15Cu–15Ni braze alloy can readily wet the Ti–6Al–4V substrate at 970 °C. It is attributed to the titanium-based Ti–15Cu–15Ni braze alloy. The dissolution of Ti–6Al–4V into the molten braze promotes the wettability of the Ti–15Cu–15Ni braze alloy.

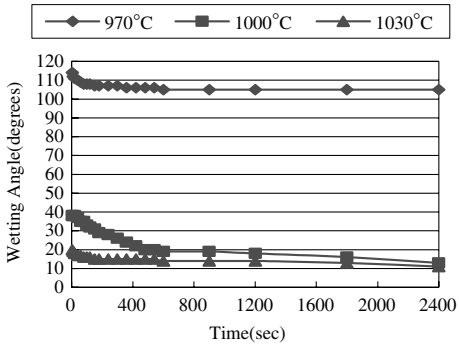

Fig. 2. Wetting angle tests of Ti–15Cu–15Ni braze alloy on the Mo substrate at various temperatures for 0–2400 s.

Fig. 2 displays the wetting angle test result of Ti–15Cu–15Ni braze alloy on the Mo substrate at 970, 1000 and 1030 °C for 0–2400 s, respectively. It is obvious that Ti–15Cu–15Ni braze alloy demonstrates poor wettability on the Mo substrate at 970 °C, and its wetting angle is as high as 103 degrees. However, the Ti–15Cu–15Ni braze alloy shows excellent wettability on the Mo substrate as the test temperature increased to 1000 °C. With increasing the test temperature, the wettability of the braze alloy is significantly improved as illustrated in the figure.

3.2. Evaluation of brazed Ti–6Al–4V/Ti–15Cu–15Ni/Mo joints

Fig. 3 shows the SEM backscattered electron images (BEIs) and EDS chemical analyses of infrared brazed specimens at different brazing conditions. According to the EDS chemical analysis results, the infrared brazed joint primarily consists of Ti-rich phase alloyed with Al, Cu, Ni, V and Mo as marked by points C–E in Fig. 3(a). Based on the phase diagrams, the β-Ti dissolves Cu and Ni up to 11 and 13 at%, respectively [3,24]. Additionally, the β-Ti is completely soluble with V and Mo, and the solubility of Al in Ti exceeds

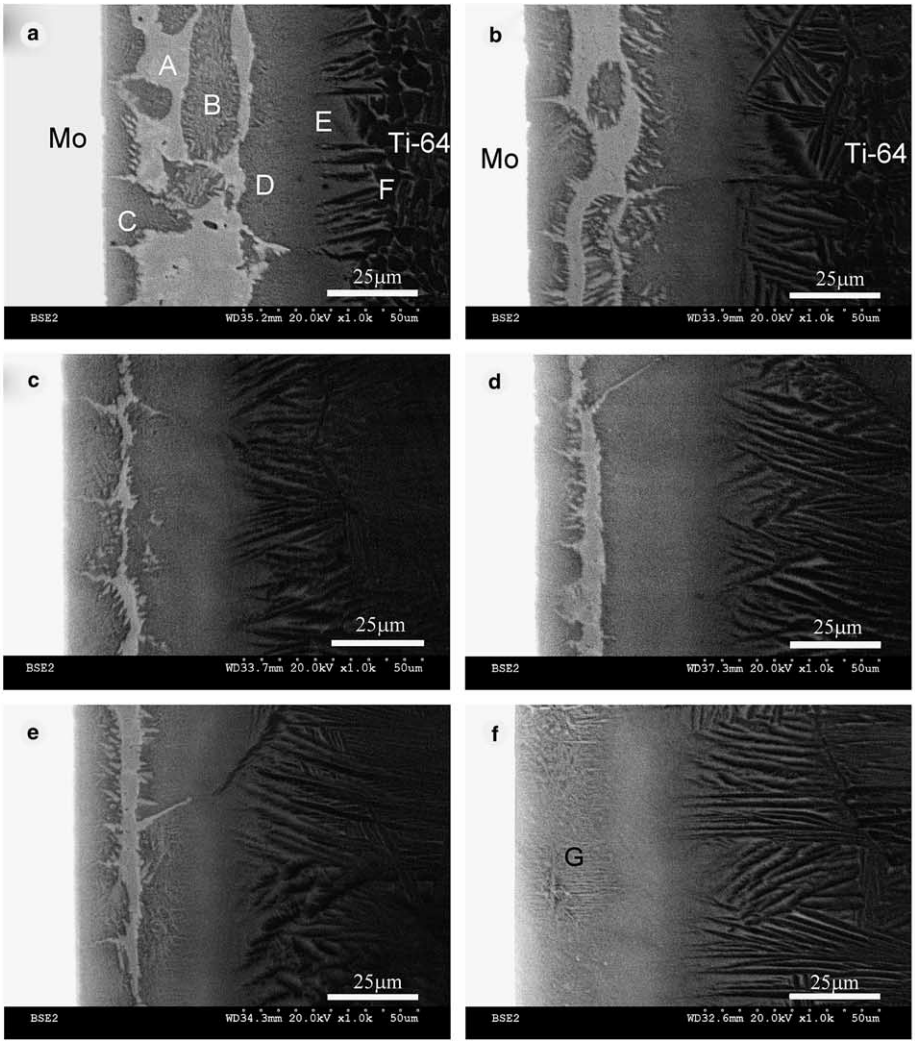

Location	A	B	C	D	E	F	G
Ti	68.7	83.2	76.8	82.9	77.6	90.7	81.1
V	0.1	1.1	0.6	0.8	4.3	1.7	1.2
Ni	15.2	6.9	8.1	7.0	6.4	0.3	5.9
Cu	14.9	5.1	9.7	6.2	6.7	0.2	6.7
Al	1.0	2.1	1.5	2.1	5.1	7.1	3.4
Mo	0.1	1.6	3.2	1.1	0.0	0.0	1.7

Fig. 3. SEM BEIs and EDS chemical analysis results of infrared brazed specimens in atomic percent with various brazing conditions: (a) 970 °C × 180 s, (b) 970 °C × 300 s, (c)1000 °C × 180 s, (d) 1000 °C × 300 s, (e) 1030 °C × 180 s and (f) 1030 °C × 300 s.

11 at% at 500 °C [3]. Accordingly, it is reasonable to conclude that Al, Cu, Ni, V and Mo are dissolved in the Ti-rich matrix. According to Fig. 3(a), point A with the highest Cu and Ni contents is caused by the fast infrared brazing history. With increase the brazing temperature and/or time, the amount of transient phase A is gradually disappeared as demonstrated in Fig. 3. Finally, the phase marked by G is observed in the infrared brazed joint as illustrated in Fig. 3(f). It is important to note that there is no interfacial reaction layer observed in the brazed joint, so the Ti–15Cu–15Ni braze alloy is very suitable in brazing Ti–6Al–4V and Mo.

Fig. 4 displays the SEM images and EDS chemical analysis results of furnace brazed specimens at 970 °C with different brazing time. Similarly, the furnace brazed joint is mainly composed of the Ti-rich phase. Both coarse platelike α-Ti and transformed β-Ti alloyed with Al, Cu, Ni, V and Mo are observed in the furnace brazed specimen. Compared with the infrared brazing, the mass transport among the molten braze and two substrates is significantly increased during furnace brazing because of its slow thermal cycle. Accordingly, the amount of Mo content in the Ti-rich phase is greatly increased in the furnace brazed joint as marked by point A

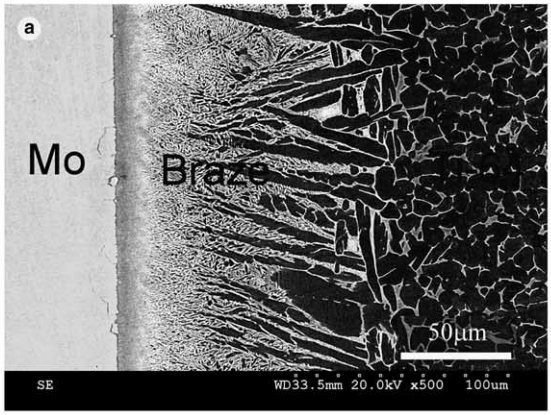

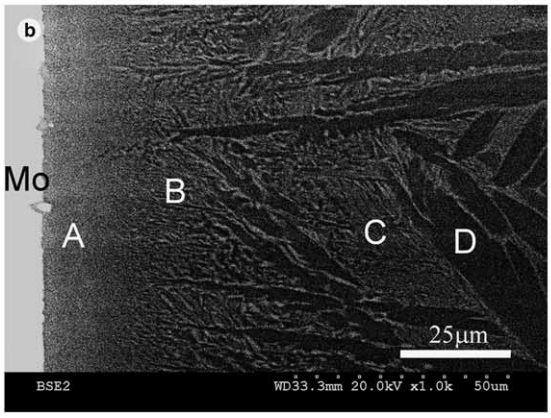

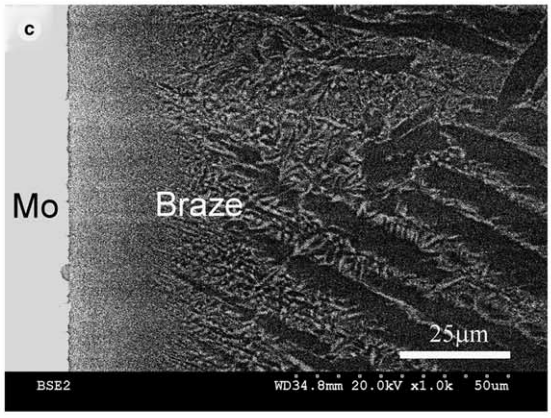

Location	A	B	C	D
Ti	77.6	82.0	83.0	87.2
V	2.5	3.4	5.0	3.8
Ni	2.0	3.1	4.3	0.5
Cu	2.2	3.7	1.9	1.0
Al	2.5	4.0	4.4	7.4
Mo	13.2	3.8	1.4	0.1

Fig. 4. The SEM images and EDS chemical analysis results of furnace brazed joints in atomic percent at 970 °C for (a) 600 s, SEI, (b) 1200 s, BEI and (c) 1800 s, BEI.

in Fig. 4. The amount of Cu and Ni contents in the furnace brazed specimen is also decreased as compared with that of infrared brazed ones (Fig. 3 and Fig. 4). Similar to the aforementioned result, no interfacial reaction layer is found in the furnace brazed joint.

Table 2 summarizes shear strengths of all brazed specimens for various brazing conditions. Most of the brazed joints are fractured at the Mo substrate except for the infrared brazed joint at 970 °C for 180 seconds. Fig. 5 shows the macroscopic cross section of the brazed joint after shear test with different brazing conditions. Fracture of the Mo substrate can be observed as marked by A in the figure, and it may be caused by two reasons. First, the strength of Mo substrate (575 MPa) is significantly lower than that of Ti–6Al–4V substrate (1200 MPa) [1,4]. Second, residual thermal stresses of the brazed joint may also play an important role in the shear test. Thermal expansion coefficients of Ti–6Al–4V and Mo at 25 °C are 8.6×10^{-6} and 4.8×10^{-6} 1/°K, respectively [1,4,25]. It is expected that there are high residual thermal stresses in the joint after brazing due to thermal expansion mismatch among Ti–6Al–4V, Mo and the braze alloy. The effect of residual stresses in the brazed joint will be analyzed in the following ABAQUS® simulations.

The average shear strength of the specimen infrared brazed at 970 °C for 180 s is 251 MPa. The cross section of the above fractured specimen is mounted in an epoxy, and examined by an SEM in order to perform failure analysis of the fractured joint. Fig. 6 shows the SEM BEI cross-section image and the fractograph of the brazed joint after shear test. It is clear that failure of the infrared brazed joint is located at the braze alloy as illustrated in Fig. 6(a). Additionally, quasi-cleavage fracture with sliding marks on facets is widely observed in the fractured surface as shown in Fig. 6(b).

3.3. ABAQUS simulation of residual stresses in the brazed joint

Fig. 7(a) displays the schematic diagram of the shear test specimen used in the experiment. Since both the residual thermal stress and applied shear stress are symmetric to the center of the specimen, a quarter model is constructed for the ABAQUS® simulation as shown in the grey area of the figure. A three-dimensional ABAQUS® model of the shear test specimen is illustrated in Fig. 7(b), and appropriate boundary conditions are placed on the quarter model. It is noted that the braze alloy, Ti–15Cu–15Ni, is located between the Mo and Ti–6Al–4V substrate throughout the analyses.

Both linear elastic and plastic models are applied in ABAQUS® simulation [20–23]. Thermal expansion coefficient, Young's modulus and Poisson's ratio are all required properties for the elastic analysis. In addition to the above properties, yield strength, tensile strength and elongation at elevated temperatures are also necessary in order to carry out plastic simulation. Because there are no sufficient experimental data available for Ti–15Cu–15Ni and Ti–6Al–4V alloys, properties of Ti are used as the first approximation in the

Table 2
Shear strengths of all brazed specimens for various brazing conditions

Brazing type	Temperature (°C)	Time (s)	Shear strength (MPa)	Average shear strength (MPa)
Furnace	970	1200 1200	Fracture of Mo substrate	
Infrared	970	180 180	254 248	251 MPa
Infrared	1000	180 180	Fracture of Mo substrate	
Infrared	1030	180 180	Fracture of Mo substrate	
Infrared	1060	180 180	Fracture of Mo substrate	

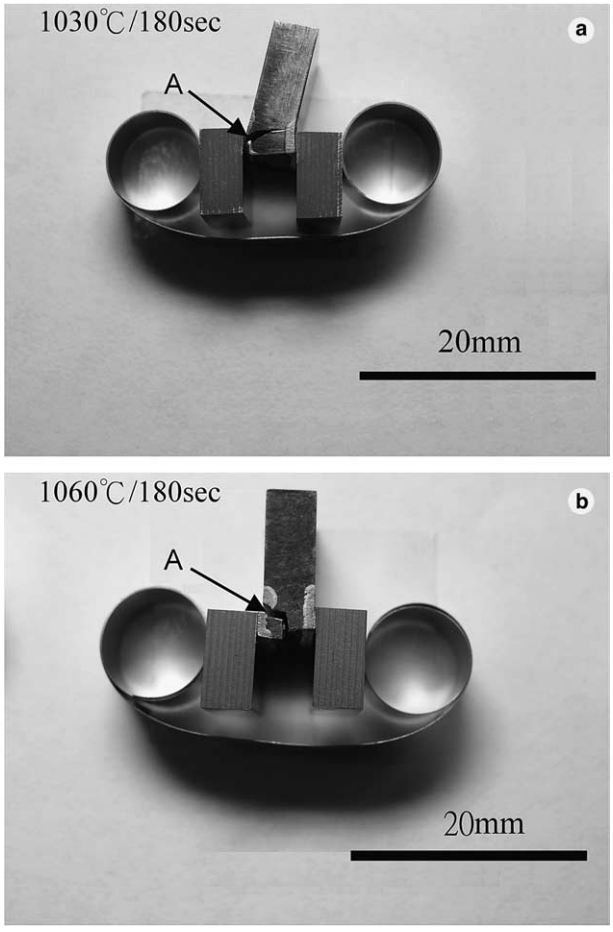

Fig. 5. The macroscopic cross section of the brazed joint after shear test: (a) 1030 °C × 180 s and (b) 1060 °C × 180 s.

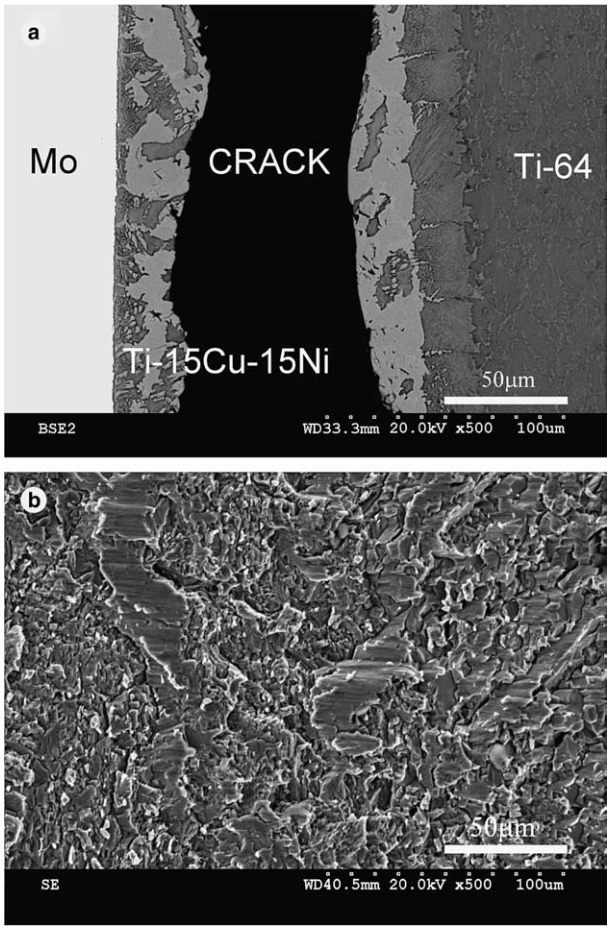

Fig. 6. SEM (a) BEI cross-sectional image and (b) SEI fractograph of the infrared brazed joint at 970 °C for 180 s after shear test.

analysis. Table 3 lists all required properties used in ABAQUS® simulations [4,25].

For the three dimensional model, six stress components (S_{11}, S_{22}, S_{33}, S_{12}, S_{13} and S_{23}), six strain components (E_{11}, E_{22}, E_{33}, E_{12}, E_{13} and E_{23}) and Mises equivalent stress are derived from the output process [20]. There are two stages in the ABAQUS® residual stress simulation. First, the residual thermal stress is developed after the specimen brazed at 970, 1000, 1030 and 1060 °C, respectively. Second, the residual stress of the brazed joint is redistributed after shear test. Both stages are sequentially simulated by ABAQUS® analysis.

For the first brazing stage, the initial temperature of the specimen is set at 970, 1000, 1030 and 1060 °C,

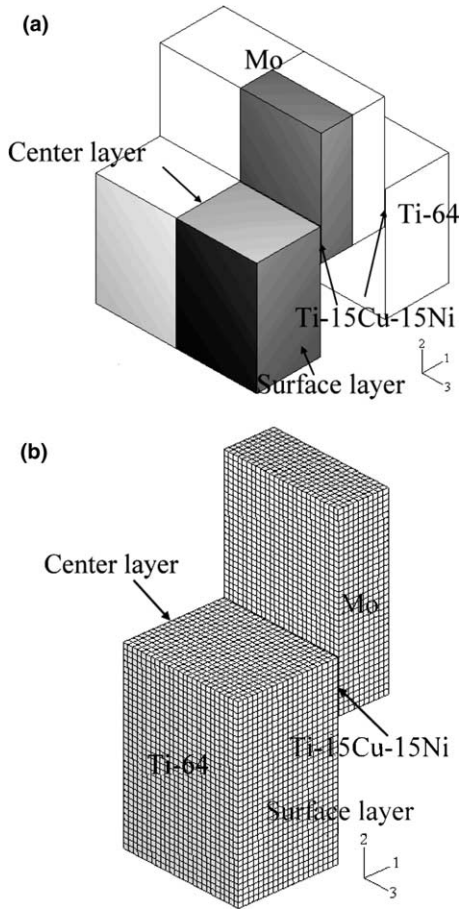

Fig. 7. (a) Schematic diagram of the shear test specimen used in the experiment, and (b) the quarter model of the shear test specimen used in ABAQUS simulation.

respectively. The final temperature of these specimens after brazing is 25 °C. Fig. 8(a) displays the Mises stress contour of the specimen after brazing at 1030 °C. The residual thermal stress is developed in the specimen, and the brazed joint has the highest Mises stress as shown in the figure. For the second shear test stage, a 250 MPa stress is tentatively applied to the brazed joint in order to simulate the residual stress of the shear test specimen. The average shear strength of infrared brazed

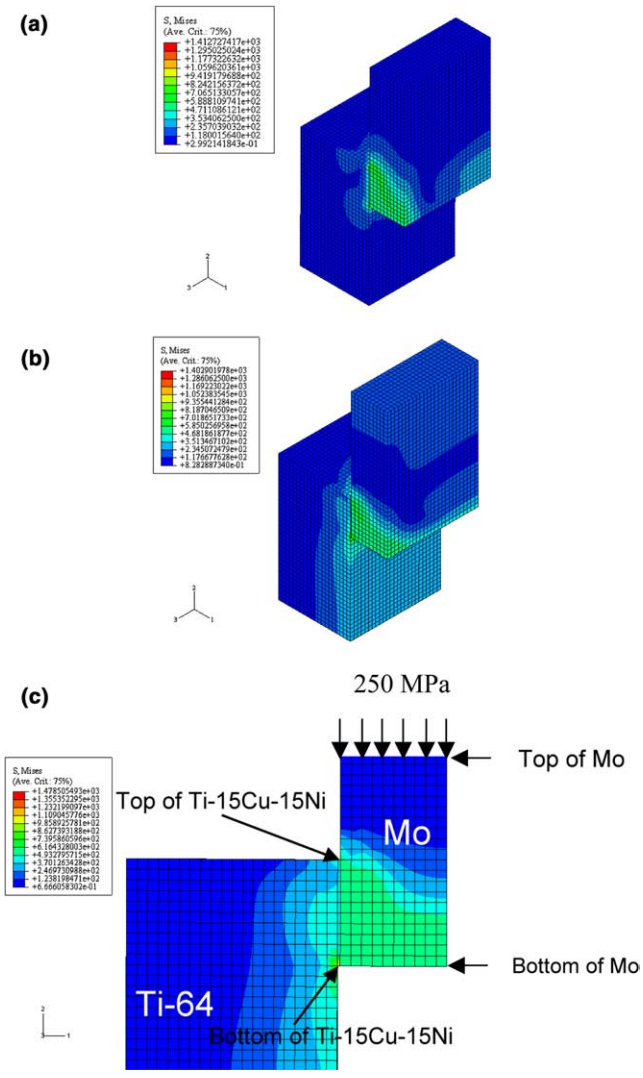

Fig. 8. The Mises stress contour of the specimen: (a) after brazing at 1030 °C, (b) the brazed specimen after 250 MPa applied stress and (c) cross section of the part (b).

joint is 251 MPa, so 250 MPa applied stress has been chosen in the simulation. Fig. 8(b) shows the Mises stress contour of the brazed specimen after 250 MPa applied stress, and the Mises stress contour in cross section

Table 3
Required properties of Ti and Mo used in ABAQUS simulation [4,25]

Properties	Ti	Mo
Young's modulus (GPa)	110	320
Poisson's ratio	0.34	0.32
Yield strength (MPa)	890 (20 °C)	490 (20 °C)
Tensile strength (MPa)	960 (20 °C), 886 (100 °C), 750 (200 °C), 700 (300 °C), 660 (400 °C), 530 (500 °C), 220 (600 °C)	575 (20 °C), 425 (127 °C), 390 (227 °C), 340 (327 °C), 300 (427 °C), 290 (527 °C), 260 (627 °C), 234 (727 °C), 166 (927 °C), 94 (1127 °C), 72 (1327 °C)
Elongation (%)	12	4.1 (20 °C), 2.4 (1000 °C), 10.3 (1100 °C), 12.5 (1200 °C)
CTE (ppm/°K)	8.6 (20 °C), 9.4 (127 °C), 9.9 (227 °C), 10.4 (327 °C),10.8 (427 °C), 11.1 (527 °C), 11.3 (627 °C), 11.5 (727 °C), 11.8 (883 °C), 11.3 (927 °C), 12.3 (1127 °C)	4.8 (20 °C), 4.9 (127 °C), 5.1 (227 °C), 5.3 (327 °C), 5.5 (427 °C), 5.7 (527 °C), 6 (627 °C), 6.2 (727 °C), 6.7 (927 °C), 7.2 (1127 °C), 7.8 (1327 °C)

of the brazed joint is also illustrated in Fig. 8(c). Based on the figure, the Mises stress in the Mo substrate is still higher than that of Ti–6Al–4V substrate.

Fig. 9 shows the residual Mises stress of the specimen after brazing. According to the figure, the effect of brazing temperature has little impact on the Mises stress of the brazed specimen. Fig. 9(a) and (b) display Mises stresses of Mo elements next to Ti–15Cu–15Ni elements. Mises stresses of Mo elements are expressed from the bottom of the Mo substrate to its top as shown in Fig. 8(c), and the length of Mo substrate is 7 mm. It is noted that the surface layer of brazed Mo substrate has the highest Mises stress up to 700 MPa as shown in Fig. 9(a). Similarly, Fig. 9(c) and (d) illustrate Mises stresses of the braze alloy, Ti–15Cu–15Ni. Mises stresses of Ti–15Cu–15Ni elements are expressed from the bottom of Ti–15Cu–15Ni to its top as shown in Fig. 8(c), and the length of the braze alloy is 2 mm (Fig. 1). Based on Fig. 9(c) and (d), both ends of the braze alloy have high Mises stresses.

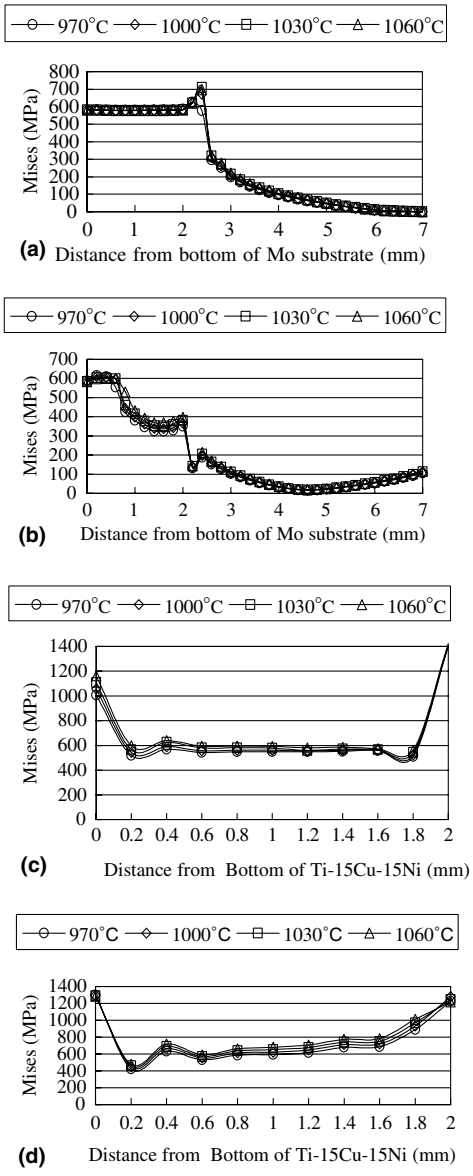

Fig. 9. Residual Mises stresses of the specimen after brazing: (a) Mo elements next to the Ti–15Cu–15Ni, the surface layer and (b) the center layer; (c) Ti–15Cu–15Ni elements, the surface layer and (d) the center layer.

Residual thermal stresses are redistributed after introducing a 250 MPa applied stress. Fig. 10 shows the Mises stress distribution of the brazed specimen after introducing a 250 MPa applied stress in the surface layer for Ti–6Al–4V, braze alloy and Mo substrate, respectively. According to the figure, the brazing temperature has little effect on the Mises stress of the shear test specimen. It is clear that the braze alloy is experienced the largest Mises stress on both ends. Accordingly, it is possible that the braze alloy is fractured during the shear test. The maximum Mises stress of Mo is about the same as that of Ti–6Al–4V. However, the tensile strength of Ti–6Al–4V is much higher than that of Mo as shown in Table 3 [4]. It is expected that the Mo substrate instead of Ti–6Al–4V is fractured during the shear test.

Fig. 11 displays the Mises stress distribution of the brazed specimen after introducing a 250 MPa applied stress in the center layer for Ti–6Al–4V, braze alloy and

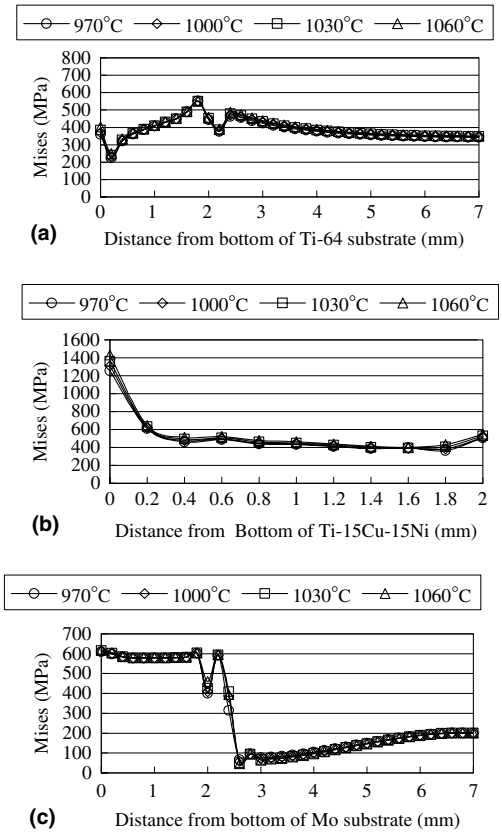

Fig. 10. The Mises stress distribution of the brazed specimen after introducing a 250 MPa applied stress in the surface layer: (a) Ti–6Al–4V substrate, (b) Ti–15Cu–15Ni braze alloy and (c) Mo substrate.

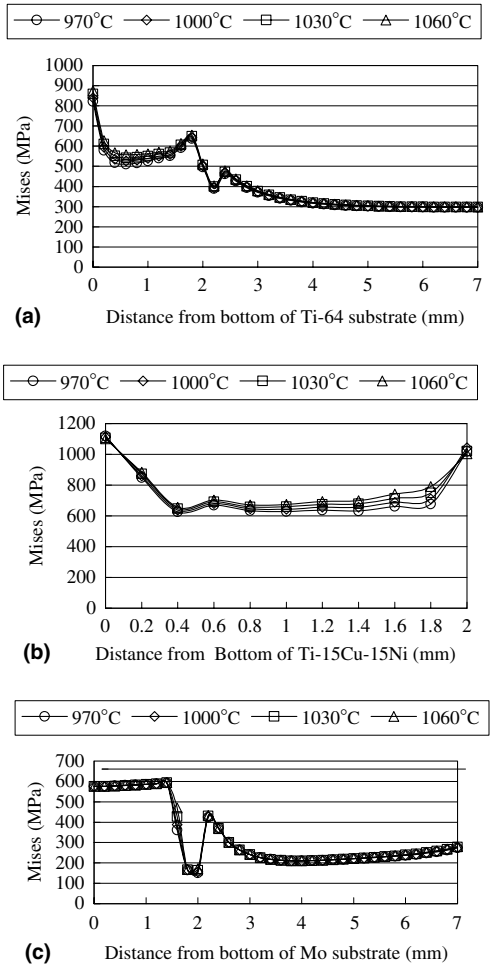

Fig. 11. The Mises stress distribution of the brazed specimen after introducing a 250 MPa applied stress in the center layer: (a) Ti–6Al–4V substrate, (b) Ti–15Cu–15Ni braze alloy and (c) Mo substrate.

Mo substrate, respectively. Similar to Fig. 10, there are two possible fracture locations in the brazed joint due to high Mises stresses, i.e., the braze alloy and Mo substrate. It is consistent with the experimental observations. The brazed joint is fractured either in the braze alloy or Mo substrate. Additionally, the inherent low strength of the Mo substrate results in premature failure of the brazed joint during the shear test for most brazed specimens.

4. Conclusions

Traditionally, the selection of braze alloys in dissimilar brazing Ti and many other alloys is difficult due to the formation of brittle interfacial reaction layer(s). In brazing dissimilar alloys, the Ti may readily react with many other elements due to its high reactivity. This research demonstrates the potential of using a commercially available Ti-based braze alloy to join Ti–6Al–4V and Mo substrates. Important conclusions are listed below:

1. The Ti-rich phase widely dominates the brazed joint, and there is no interfacial reaction layer in the brazed joint, especially for the interface between the Mo and braze alloy. Accordingly, the use of titanium-based braze alloys may be also suitable for (infrared) brazing many other titanium alloys and refractory metals, and it can be further studied in the future.
2. Based on the experimental observations, Ti–15Cu–15Ni molten braze exhibits excellent wettability on the Ti–6Al–4V substrate. In contrast, Ti–15Cu–15Ni braze alloy demonstrates poor wettability on the Mo substrate at 970 °C. Its wettability on the Mo substrate is greatly improved for test temperatures above 1000 °C.
3. Ti–6Al–4V and Mo substrates can be successfully brazed using the Ti–15Cu–15Ni filler metal. Most of the brazed joints are fractured at the Mo substrate except for the joint infrared brazed at 970 °C for 180 s. The average shear strength of the specimen infrared brazed at 970 °C for 180 s is 251 MPa. The failure of the joint is located at the braze alloy, and quasi-cleavage fracture with sliding marks on facets is widely observed on the fractured surface.
4. Based on the ABAQUS simulated result, there are two possible fracture locations in the brazed joint due to the presence of high Mises stresses, i.e., the braze alloy and Mo substrate. Additionally, the inherent low strength of the Mo substrate results in premature failure of the brazed joint during shear test for most brazed specimens.

Acknowledgements

The authors gratefully acknowledge the financial support of this research by the National Science Council (NSC), Republic of China under NSC grant 93-2216-E-002-028.

References

[1] Smith WF. Structure and properties of engineering alloys. New York: McGraw-Hill Inc; 1993.
[2] Collins PC, Banerjee R, Banerjee S, Fraser HL. Laser deposition of compositionally graded titanium–vanadium and titanium–molybdenum alloys. Mater Sci Eng A 2003;352:118–28.
[3] Massalski TB. Binary alloy phase diagrams. Materials Park: ASM International; 1990.
[4] Davis JR, editor. Metals handbook, properties and selection: nonferrous alloys and special purpose materials, vol. 2. Materials Park: ASM International; 1990.
[5] Schwartz M. Brazing. Materials Park: ASM International; 1987. p. 77–80.
[6] Schwartz M. Brazing: for the engineering technologist. Materials Park: ASM International; 1995. p. 172–4.
[7] Olson DL, Siewert TA, Liu S, Edwards GR, editors. ASM handbook, welding, brazing and soldering. Materials Park: ASM International; 1993.

[8] Humpston G, Jacobson DM. Principles of soldering and brazing. Materials Park: ASM International; 1993.
[9] Lee YL, Shiue RK, Wu SK. The microstructural evolution of infrared brazed Fe_3Al by BNi-2 braze alloy. Intermetallics 2003;11(3):187–95.
[10] Shiue RK, Wu SK, Hung CM. Infrared repair brazing of 403 stainless steel with a nickel based braze alloy. Metall Mater Trans 2002;33A(6):1765–73.
[11] Yang TY, Wu SK, Shiue RK. Interfacial reaction of infrared brazed NiAl/Al/NiAl and Ni_3Al/Al/Ni_3Al joints. Intermetallics 2001;9(4):341–7.
[12] Shiue RK, Wu SK, Chen SY. Infrared brazing of TiAl intermetallic using BAg-8 braze alloy. Acta Mater 2003;51(7):1991–2004.
[13] Chan HY, Liaw DW, Shiue RK. The microstructural observation of brazing Ti–6Al–4V and TZM using the BAg-8 braze alloy. Int J Refract Metal Hard Mater 2004;22:27–33.
[14] Yang TY, Shiue RK, Wu SK. Infrared brazing of $Ti_{50}Ni_{50}$ using pure Cu and Ti–15Cu–15Ni foils. Intermetallics 2004;12(12): 1285–92.
[15] Ou CL, Shiue RK. Microstructural evolution of brazing 422 stainless steel using the BNi-3 braze alloy. J Mater Sci 2003; 38(11):2337–46.
[16] Liu CC, Ou CL, Shiue RK. The microstructural observation and wettability study of brazing Ti–6Al–4V and 304 stainless steel using three braze alloys. J Mater Sci 2002;37(11):2225–35.
[17] Vander Voort GF. Metallography principle and practice. New York: McGarw-Hill Inc.; 1984.
[18] Hiraoka Y. Brazing of single-crystalline molybdenum by using Pd–20% Ag alloy. Int J Refract Metal Hard Mater 1992;11: 303–7.
[19] Hiraoka Y, Nishikawa S. Joining of single crystal Mo and carbonceramics by using Pd and Pd–Ag alloy as brazing metal. Int J Refract Metal Hard Mater 1996;14:311–7.
[20] Hibbitt B, Karlsson B, Sorensen P. ABAQUS/standard user's manual. Rode Island: Hibbitt, Karlsson & Sorensen Inc.; 2001.
[21] Tsay LW, Lin ZW, Shiue RK, Chen C. Hydrogen embrittlement susceptibility of laser-hardened 4140 steel. Mater Sci Eng A 2000;A290:46–54.
[22] Zhuang WD, Chang PC, Chou FY, Shiue RK. Effect of solder creep on the reliability of large area die attachment. Microelectron Reliab 2001;41:2011–21.
[23] Shiue RK, Chang CT, Young MC, Tsay LW. The effect of residual thermal stresses on the fatigue crack growth of laser-surface-annealed AISI 304 stainless steel—part I: computer simulation. Mater Sci Eng A 2004;A364:102–9.
[24] Villars P, Prince A, Okamoto H. Handbook of ternary alloy phase diagrams. Materials Park: ASM International; 1995.
[25] Touloukian YS, Kirby RK, Taylor RE, Lee TYR. Thermal physical properties of matter. New York: IFI/Plenum Press; 1977.